Synthesis, Structural Characterization, and Luminescence Properties of Lanthanide Oxalatophosphonates: $Na[M_3(H_2O)_4(C_2O_4)_4(CH_3PO_3)]\cdot 2H_2O$ (M = Nd and Pr)

Ya-Ling Huang,[†] Meow-Yu Huang,[†] Tsung-Han Chan,[†] Bor-Chen Chang,*[,†] and Kwang-Hwa Lii*[,†,‡]

Department of Chemistry, National Central University, Chungli, Taiwan, and Institute of Chemistry, Academia Sinica, Taipei, Taiwan

Received March 3, 2007. Revised Manuscript Received April 17, 2007

A neodymium oxalatophosphonate and its praseodymium analogue, $Na[Nd_3(H_2O)_4(C_2O_4)_4(CH_3PO_3)]\cdot 2H_2O$ and $Na[Pr_3(H_2O)_4(C_2O_4)_4(CH_3PO_3)]\cdot 2H_2O$, have been synthesized by a hydrothermal method and characterized by single-crystal X-ray diffraction and thermogravimetric analysis. We studied the photoluminescence spectra of the Nd and Pr compounds as well as the magnetic properties of the Nd compound. The structure consists of layers built of tetramers of edge- and face-sharing NdO_9 (or PrO_9) polyhedra connected by oxalate and methylphosphonate units, which are linked by zigzag infinite chains of oxalate-bridged NdO_9 (or PrO_9) polyhedra to form a 3D framework. They are the first examples of lanthanide oxalate-methylphosphonate. The Nd compound displays characteristic emission bands in the near IR region. The $\chi_M T$ value decreases from 1.68 cm^3 K/mol Nd at 300 K to 0.659 cm^3 K/mol Nd at 2 K. The value at room temperature is close to the theoretical value for a mononuclear Nd^{3+} species. Luminescence of the Pr compound consists of many emission bands at 480−760 nm. The lifetimes of both compounds are much shorter than the expected values because of the quenching effects of water molecules in the structure. Crystal data for the Nd compound: triclinic, $P\bar{1}$ (No. 2), $a = 9.0682(2)$ Å, $b = 9.5114(3)$ Å, $c = 14.0066(4)$ Å, $\alpha = 74.975(2)°$, $\beta = 86.534(2)°$, $\gamma = 82.725(2)°$, and $Z = 2$. Crystal data for the Pr compound are the same as those for the Nd compound, except $a = 9.125(1)$ Å, $b = 9.549(1)$ Å, $c = 14.073(2)$ Å, $\alpha = 75.086(2)°$, $\beta = 86.611(2)°$, and $\gamma = 82.545(2)°$.

Introduction

There have been considerable interests in the synthesis of open-framework metal phosphates because of their interesting structural chemistry and potential applications.[1−3] Recently, many research activities have focused on the synthesis of hybrid frameworks by incorporating organic ligands in the structures of metal phosphates. Among the large number of carboxylates compounds, the oxalate moiety, $C_2O_4^{2-}$, was found to be a good candidate and has been successfully incorporated into phosphate frameworks with transition metals and main group elements.[4] However, few reports in the literature illustrate the use of oxalate anion forming part of the structure along with the phosphonate groups, although the chemistry of metal phosphonates has been extensively studied for many years.[5] $Sn_2(O_3PCH_3)(C_2O_4)$ and $Sn_4(O_3PCH_2CH_2CO_2)_2(C_2O_4)$ are the first members of metal oxalatophosphonates.[6,7] The former has a layer structure, and the latter adopts a 3D framework structure that consists of two different bifunctional linkers, phosphonopropionate and oxalate anions. Other examples include the first organically templated metal oxalatophosphonate with a layer structure, $(C_3H_{12}N_2)_{0.5}[Ga_3(C_2O_4)(CH_3PO_3)_4]\cdot 0.5H_2O$,[8] and several lanthanide oxalate-aminophosphonate hybrids with 3D framework structures.[9] All of these oxalatophosphonates were synthesized in aqueous solutions under hydrothermal conditions. Recently, we synthesized a new iron(II) oxalatophosphonate, $Na_2Fe_3(C_2O_4)_3(CH_3PO_3H)_2$, and the manganese analogue by using a low-melting-point eutectic mixture of choline chloride and malonic

* Corresponding author. E-mail: liikh@cc.ncu.edu.tw (K.-H.L); bchang@cc.ncu.edu.tw (B.-C.C.).
[†] National Central University.
[‡] Academia Sinica.

(1) Haushalter, R. C.; Mundi, L. A. *Chem. Mater.* **1992**, *4*, 31.
(2) Lii, K.-H.; Huang, Y.-F.; Zima, V.; Huang, C.-Y.; Lin, H.-M.; Jiang, Y.-C.; Liao, F.-L.; Wang, S.-L. *Chem. Mater.* **1998**, *10*, 2599.
(3) Cheetham, A. K.; Ferey, G.; Loiseau, T. *Angew. Chem., Int. Ed.* **1999**, *38*, 3268.
(4) (a) Lin, H.-M.; Lii, K.-H.; Jiang, Y.-C.; Wang, S.-L. *Chem. Mater.* **1999**, *11*, 519. (b) Lethbridge, Z. A. D.; Lightfoot, P. *J. Solid State Chem.* **1999**, *143*, 58. (c) Choudhury, A.; Natarajan, S.; Rao, C. N. R. *J. Solid State Chem.* **1999**, *146*, 538. (d) Hung, L.-C.; Kao, H.-M.; Lii, K.-H. *Chem. Mater.* **2000**, *12*, 2411. (e) Do, J.; Bontchev, R. P.; Jacobson, A. J. *Chem. Mater.* **2001**, *13*, 2601. (f) Choi, C. T. S.; Anokhina, E. V.; Day, C. S.; Zhao, Y.; Taulelle, F.; Huguenard, C.; Gan, Z.; Lachgar, A. *Chem. Mater.* **2002**, *14*, 4096. (g) Jiang, Y.-C.; Wang, S.-L.; Lii, K.-H.; Nguyen, N.; Ducouret, A. *Chem. Mater.* **2003**, *15*, 1633. (h) Loiseau, T.; Férey, G.; Haouas, M.; Taulelle, F. *Chem. Mater.* **2004**, *16*, 5318. (i) Chang, W.-M.; Wang, S.-L. *Chem. Mater.* **2005**, *17*, 74. (j) Sheu, C.-Y.; Lee, S.-F.; Lii, K.-H. *Inorg. Chem.* **2006**, *45*, *1891*.
(5) (a) Clearfield, A. Metal Phosphonate Chemistry. In *Progress in Inorganic Chemistry*; Karlin, K. D., Ed.; John Wiley & Sons: New York, 1998; Vol. 47, pp 371−510. (b) Clearfield, A. *Curr. Opin. Solid State Mater. Sci.* **2002**, *6*, 495 and references therein.
(6) Adair, B.; Natarajan, S.; Cheetham, A. K. *J. Mater. Chem.* **1998**, *8*, 1477.
(7) Stock, N.; Stucky, G. D.; Cheetham, A. K. *Chem. Commun.* **2000**, 2277.
(8) Lin, C.-H.; Lii, K.-H. *Inorg. Chem.* **2004**, *43*, 6403.
(9) Song, J.-L.; Mao, J.-G. *Chem.—Eur. J.* **2005**, *11*, 1417.

10.1021/cm070602i CCC: $37.00
Published on Web 05/31/2007

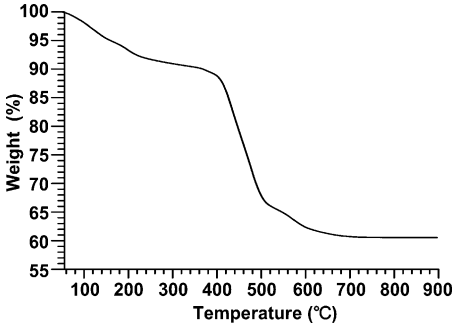

Figure 1. Thermogravimetric analysis of **1** in flowing oxygen at 5 °C min^{-1}.

acid as a solvent.[10] Several organically templated metal oxalatophosphites have also been reported.[11] We are currently investigating the synthesis of rare earth compounds because of their interesting structural chemistry and photoluminescence properties. One noticeable difference between transition metal and lanthanide ions is the tendency toward increased coordination numbers in the lanthanide complexes. This is shown most readily by the early members of the lanthanide series. Lanthanide-containing compounds are interesting luminescence materials because they emit over the entire spectral range: near-infrared (Nd^{3+}, Er^{3+}), red (Eu^{3+}, Pr^{3+}, Sm^{3+}), green (Er^{3+}, Tb^{3+}), and blue (Tm^{3+}, Ce^{3+}).[12] In this contribution, we describe the hydrothermal synthesis and structural characterization by single-crystal X-ray diffraction of a new neodymium oxalatophosphonate, $Na[Nd_3(H_2O)_4(C_2O_4)_4(CH_3PO_3)]\cdot 2H_2O$ (denoted as **1**), and the praseodymium analogue (denoted as **2**) that have a novel 3D framework structure built of a discrete NdO_9 (or PrO_9) polyhedron, a tetramer of edge- and face-sharing NdO_9 (or PrO_9) polyhedra, in addition to a methylphosphonate group and six distinct oxalate units. The photoluminescence properties of both compounds and the magnetic properties of **1** have also been studied.

Experimental Section

Synthesis. Light-violet block crystals of **1** were obtained as the only solid product by heating a mixture of $Nd(NO_3)_3\cdot 6H_2O$ (0.1315 g, 0.3 mmol), $Na_2C_2O_4$ (0.0536 g, 0.4 mmol), methylphosphonic acid (0.0096 g, 0.1 mmol), NaOH(aq) (5 M, 30 μL), and H_2O (8 mL) in a Teflon-lined 23 mL autoclave at 165 °C for 3 days, followed by slow cooling at 6 °C/h to room temperature. The pH values of the solution before and after the hydrothermal reaction were 7.6 and 5.2, respectively. Energy-dispersive X-ray fluorescence spectroscopic analysis of several crystals confirms the presence of Na, P, and Nd. The purity of the sample for property measurements was checked by powder X-ray diffraction (see Figure S1 in the Supporting Information). Elemental analysis results are consistent with the formula (Anal. Found (calcd): C, 10.53 (10.70); H, 1.85 (1.50)). The yield was 82% based on Nd. Thermogravimetric analysis was carried out from room temperature to 900 °C in flowing O_2 at 5 °C min^{-1} (Figure 1). The final decomposition products were $Nd_3(PO_4)O_3$ (JCPDS 33-938) and Na_2O (JCPDS 23-528) identified by powder X-ray diffraction. The first step (50−380 °C) corresponds to the loss of six water molecules (obsd. 10.4%; six H_2O calcd., 10.69%). The steps between 380 and 700 °C can be attributed to decomposition of oxalate and phosphonate units. The observed total weight loss (39.46%) agrees well with the calculated value of 39.90% according to the following equations.

$$Na[Nd_3(H_2O)_4(C_2O_4)_4(CH_3PO_3)]\cdot 2H_2O \xrightarrow{-6H_2O} \text{'}Na[Nd_3(C_2O_4)_4(CH_3PO_3)]\text{'}$$

$$Na[Nd_3(C_2O_4)_4(CH_3PO_3)] \xrightarrow{-4(CO+CO_2)} NaNd_3(CH_3PO_3)O_4$$

$$NaNd_3(CH_3PO_3)O_4 + 2O_2 \xrightarrow{-(1.5H_2O+CO_2)} Nd_3(PO_4)O_3 + 0.5Na_2O$$

The XRD pattern of a sample that has been heated at 300 °C in air for several hours shows that the structure of **1** is decomposed and the product is amorphous.

Compound **2** was prepared by heating a mixture of $Pr(NO_3)_3\cdot 5H_2O$ (0.1251 g, 0.3 mmol), $Na_2C_2O_4$ (0.0536 g, 0.4 mmol), methylphosphonic acid (0.0096 g, 0.1 mmol), NaOH(aq) (5 M, 40 μL), and H_2O (8 mL) in a Teflon-lined 23-mL autoclave under the same reaction conditions as those for the Nd compound. Green tablet crystals of **2** as the major product and a small amount of unidentified side product, as indicated from powder X-ray diffraction (see Figure S2 in the Supporting Information), were obtained. The largest peak of the impurity phase in the diffraction pattern is about 3% of that for **2**. An EDX analysis of a few green crystals confirms the presence of Na, P, and Pr. Elemental analysis of a sample of manually selected green crystals was also performed (Anal. Found (calcd): C, 10.89 (10.81); H, 1.98 (1.51)). An optimum set of reaction conditions to prepare a single-phase product of **2** has not been found. The TGA curve for **2** is similar to that for **1** (see Figure S3 in the Supporting Information). The processes of thermal decomposition of the two compounds are presumably the same.

Physical Measurements. Variable-temperature magnetic susceptibility χ(T) data were obtained on 32.5 mg of a polycrystalline sample of **1** from 2 to 300 K in a magnetic field of 3 kG after zero-field cooling using a Quantum Design SQUID magnetometer. Correction for diamagnetism was made according to Selwood.[13] For the photoluminescence study, a powder sample of **1** was contained between two pieces of quartz glass plates. A continuous wave (cw) laser beam at 514.5 nm was adopted as the light source to excite the sample for recording the emission spectrum. The near-infrared (NIR) emission was collected and imaged onto a monochromator (SPEX Model 500M) attached with a UV enhance Ge (North Coast Model EO-817L) detector. For the photoluminescence study of compound **2**, several manually selected green crystals of **2** were contained in a glass capillary and excited by a 473 nm cw laser beam. The emission was collected by an f/1 focal lens and imaged onto a monochromator (Acton Research Corporation SP2300i) attached with a charge-coupled device (CCD, Andor DV 401A-BV) detector. This setup was also used for the measurements of emission radiative lifetime except the detector and the light source were replaced by a photomultiplier tube (PMT, Hamamatsu R636−10) and a tunable pulsed Nd:YAG laser (Spectra Physics INDI-40-10) pumped dye laser (Lambda Physik Scanmate 2E) beam, respectively.

(10) Tsao, C.-P.; Sheu, C.-Y.; Nguyen, N.; Lii, K.-H. *Inorg. Chem.* **2006**, *45*, 6361.
(11) (a) Mandal, S.; Natarajan, S. *J. Solid State Chem.* **2005**, *178*, 2376. (b) Mandal, S.; Pati, S. K.; Green, M. A.; Natarajan, S. *Chem. Mater.* **2005**, *17*, 2912. (c) Mandal, S.; Green, M. A.; Pati, S. K.; Natarajan, S. *J. Mater. Chem.* **2007**, *17*, 980. (d) Mandal, S.; Natarajan, S. *Chem.—Eur. J.* **2007**, *13*, 968.
(12) Rocha, J.; Carlos, L. D. *Curr. Opin. Solid State Mater. Sci.* **2003**, *7*, 199.
(13) Selwood, P. W. *Magnetochemistry*; Interscience: New York, 1956.

Table 1. Crystallographic Data for $Na[Nd_3(H_2O)_4(C_2O_4)_4(CH_3PO_3)]\cdot 2H_2O$ (1) and $Na[Pr_3(H_2O)_4(C_2O_4)_4(CH_3PO_3)]\cdot 2H_2O$ (2)

	1	2
formula	$C_9H_{15}O_{25}NaNd_3P$	$C_9H_{15}O_{25}NaPPr_3$
a (Å)	9.0682(2)	9.125(1)
b (Å)	9.5114(3)	9.549(1)
c (Å)	14.0066(4)	14.073(2)
α (deg)	74.975(2)	75.086(2)
β (deg)	86.534(2)	86.611(2)
γ (deg)	82.725(2)	82.545(2)
V (Å^3)	1156.90(6)	1174.6(4)
Z	2	2
fw	1009.89	999.90
space group	$P\bar{1}$	$P\bar{1}$
T (K)	296	296
λ(Mo Kα) (Å)	0.71073	0.71073
D_{calcd} (g cm^{-3})	2.882	2.827
μ(Mo Kα) (cm^{-1})	106.2	63.3
R_1[a]	0.0172	0.0308
wR_2[b]	0.0353	0.0681

[a] $R_1 = \sum||F_o| - |F_c||/\sum|F_o|$. [b] $wR_2 = [\sum w(F_o^2 - F_c^2)^2/\sum w(F_o^2)^2]^{1/2}$, $w = 1/[\sigma^2(F_o^2) + (aP)^2 + bP]$, $P = [\max(F_o^2,0) + 2(F_c)^2]/3$, where $a = 0.0141$ and $b = 0$ for **1** and $a = 0.0233$ and $b = 0$ for **2**.

Table 2. Selected Bond Lengths (Å) for $Na[Nd_3(H_2O)_4(C_2O_4)_4(CH_3PO_3)]\cdot 2H_2O$ (1) and $Na[Pr_3(H_2O)_4(C_2O_4)_4(CH_3PO_3)]\cdot 2H_2O$ (2)

Compd **1**			
Nd(1)−O(1)	2.320(2)	Nd(1)−O(2)	2.467(2)
Nd(1)−O(5)	2.484(2)	Nd(1)−O(6)	2.486(2)
Nd(1)−O(9)	2.589(2)	Nd(1)−O(14)	2.551(2)
Nd(1)−O(15)	2.539(2)	Nd(1)−Ow(1)	2.578(2)
Nd(1)−Ow(2)	2.487(2)	Nd(2)−O(2)	2.497(2)
Nd(2)−O(3)	2.384(2)	Nd(2)−O(3)	2.528(2)
Nd(2)−O(9)	2.508(2)	Nd(2)−O(10)	2.540(2)
Nd(2)−O(12)	2.494(2)	Nd(2)−O(13)	2.510(2)
Nd(2)−O(15)	2.611(2)	Nd(2)−Ow(3)	2.502(2)
Nd(3)−O(4)	2.499(2)	Nd(3)−O(7)	2.417(2)
Nd(3)−O(8)	2.527(2)	Nd(3)−O(11)	2.526(2)
Nd(3)−O(16)	2.487(2)	Nd(3)−O(17)	2.444(2)
Nd(3)−O(18)	2.457(2)	Nd(3)−O(19)	2.494(2)
Nd(3)−Ow(4)	2.479(2)	P(1)−O(1)	1.497(2)
P(1)−O(2)	1.545(2)	P(1)−O(3)	1.560(2)
P(1)−C(9)	1.788(3)		
Compd **2**			
Pr(1)−O(1)	2.336(4)	Pr(1)−O(2)	2.487(3)
Pr(1)−O(5)	2.504(4)	Pr(1)−O(6)	2.503(4)
Pr(1)−O(9)	2.614(4)	Pr(1)−O(14)	2.568(4)
Pr(1)−O(15)	2.569(4)	Pr(1)−Ow(1)	2.615(4)
Pr(1)−Ow(2)	2.532(4)	Pr(2)−O(2)	2.514(4)
Pr(2)−O(3)	2.402(3)	Pr(2)−O(3)	2.552(3)
Pr(2)−O(9)	2.518(4)	Pr(2)−O(10)	2.554(4)
Pr(2)−O(12)	2.515(4)	Pr(2)−O(13)	2.520(4)
Pr(2)−O(15)	2.622(3)	Pr(2)−Ow(3)	2.533(4)
Pr(3)−O(4)	2.521(4)	Pr(3)−O(7)	2.440(4)
Pr(3)−O(8)	2.547(4)	Pr(3)−O(11)	2.545(3)
Pr(3)−O(16)	2.496(4)	Pr(3)−O(17)	2.460(4)
Pr(3)−O(18)	2.481(4)	Pr(3)−O(19)	2.513(4)
Pr(3)-Ow(4)	2.510(4)	P(1)−O(1)	1.500(4)
P(1)−O(2)	1.544(3)	P(1)−O(3)	1.553(4)
P(1)−C(9)	1.762(6)		

Single-Crystal X-ray Diffraction. A light-violet crystal of dimensions 0.05 × 0.09 × 0.13 mm^3 for **1** and a green crystal of dimensions 0.04 × 0.08 × 0.12 mm^3 for **2** were selected for indexing and intensity data collection on a Siemens SMART CCD diffractometer equipped with a normal focus, 3-kW sealed tube X-ray source. Intensity data were collected at room temperature in 1271 frames with *ω* scans (width 0.30° per frame). The program SADABS was used for the absorption correction ($T_{min}/T_{max} = 0.722/0.952$ for **1** and 0.687/0.954 for **2**). On the basis of statistical analysis of intensity distribution and successful solution and refinement of the structure, the space groups were determined to be $P\bar{1}$ (No. 2) for both compounds. The structures were solved by direct methods and difference Fourier syntheses. All H atoms in **1** were located on difference Fourier maps. Those H atoms of the water molecules in **2** were not located. The final cycles of least-squares refinement including atomic coordinates and anisotropic thermal parameters for all non-hydrogen atoms and fixed atomic coordinates and isotropic thermal parameters for all H atoms converged at R1 = 0.0172, wR2 = 0.0353, and $S = 0.902$ for **1** and R1 = 0.0308, wR2 = 0.0681, and $S = 0.981$ for **2**. $\Delta\rho_{max,\ min} = 1.00, -0.67$ e Å^{-3} for **1** and 1.55, −0.98 e Å^{-3} for **2**. All calculations were performed using the SHELXTL version 5.1 software package.[14]

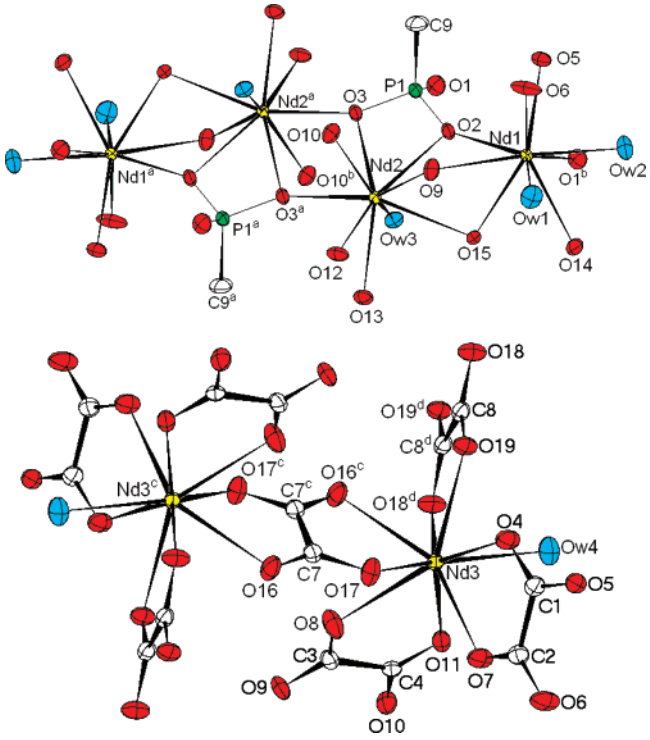

Figure 2. Building units of **1** showing atom-labeling scheme. Thermal ellipsoids are shown at the 50% probability level. Symmetry code: (a) $1 + x, -1 + y, -z$; (b) $1 + x, y, z$; (c) $x, 1 + y, z$; (d) $1 - x, -y, 1 - z$.

Results and Discussion

Structure. The crystallographic data are given in Table 1 and selected bond lengths in Table 2. The structure of **1** is constructed from the following structural elements: 3 distinct Nd−O polyhedra, 6 oxalate units, 1 CH_3PO_3 pseudotetrahedron, and 1 Na^+ ion. All atoms are in general positions. The dihedral angles in $C(1)C(2)O_4$ and $C(3)C(4)O_4$ are 175.8 and 177.1°, respectively. All other oxalate units have a center of symmetry. In all cases the Nd is 9-fold coordinated in the 3+ oxidation state as indicated by bond valence calculations,[15] and each NdO_9 unit approximates to a tricapped trigonal prism, which is a common stereochemistry for lanthanide ions. The coordination spheres of all Nd atoms are completed by water molecules, indicated by the low bond valences of the water oxygen atoms. Each $Nd(2)O_9$ polyhedron shares an edge with another $Nd(2)O_9$ and a face with a $Nd(1)O_9$ to form a tetrameric building unit, illustrated in Figure 2. These building units are linked to each other by

(14) Sheldrick, G. M. *SHELXTL Programs*, version 5.1; Bruker AXS GmbH: Karlsruhe, Germany, 1998.
(15) Brown, I. D.; Altermatt, D. *Acta Crystallogr., Sect. B* **1985**, *41*, 244.

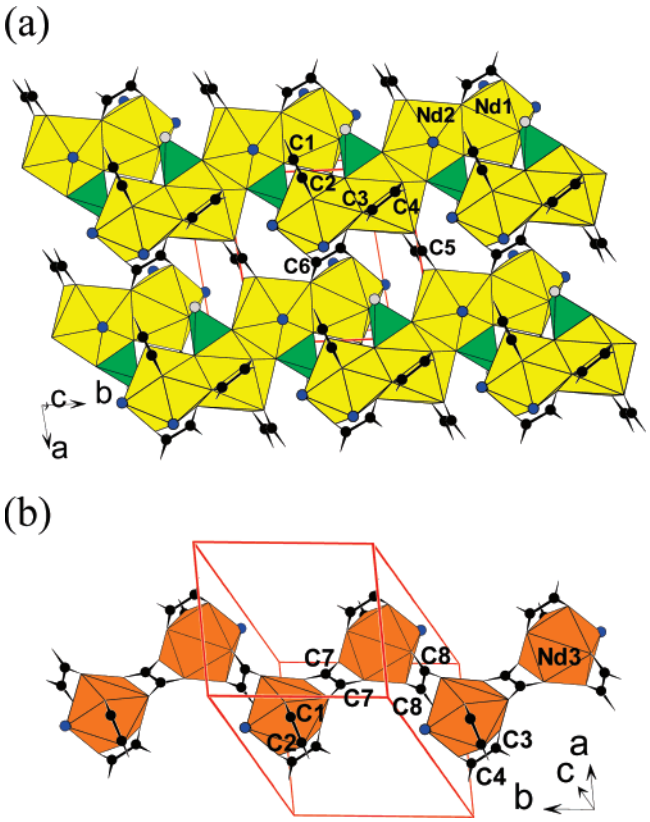

Figure 3. (a) Slice of the structure of **1** showing the connectivity between the tetramers. (b) Section of a zigzag chain formed of $Nd(3)O_9$ polyhedra linked by oxalate ligands. Key: yellow polyhedra, $Nd(1)O_9$ and $Nd(2)O_9$; brown polyhedra, $Nd(3)O_9$; green tetrahedra, methylphosphonate; blue circles, water O atoms.

$C(5)_2O_4$ and $C(6)_2O_4$ units and CH_3PO_3 tetrahedra to form neodymium oxalatophosphonate layers in the *ab* plane (Figure 3a). $Nd(3)O_9$ polyhedra are linked to each other by $C(7)_2O_4$ and $C(8)_2O_4$ units to form zigzag infinite chains along the *b*-axis (Figure 3b), which are connected to the layers by $C(1)C(2)O_4$ and $C(3)C(4)O_4$ units to form a 3D framework with small intersecting channels along the *a* and *b* axes where the Na^+ cations and the lattice water molecules (Ow(5) and Ow(6)) are located (Figure 4). The coordination number of Na^+ can be determined by the maximum cation−anion distance according to Donnay and Allmann.[16] Therefore, Na(1) is coordinated by seven oxygen atoms including three water molecules and four oxalate oxygen atoms. The bond-valence sum for Na(1) is 0.977. Extensive hydrogen bonding exists between the lattice water molecules and between the aqua molecules and framework oxygen atoms, as indicated from many Ow···Ow and Ow···O distances shorter than 2.8 Å.

All oxalate units except $C(6)_2O_4$ and $C(3)C(4)O_4$ show only bis-bidentate coordination to two Nd^{3+} ions (Figure 5a). The $C(6)_2O_4$ unit sits on an inversion center and is a bis-bidentate ligand to two Nd(1) ions as well as a bis-monodentate ligand to two Nd(2) ions (Figure 5b). Bis-monodentate and bis-bidentate coordination by the same oxalate ligand has been observed in $(C_4H_{12}N_2)[Fe^{II}_4(C_2O_4)_3(HPO_4)_2]$,[4a] $Fe^{II}_4(PO_4)_2(C_2O_4)(H_2O)_2$,[4b] and $Na_2M_3(C_2O_4)_3(CH_3PO_3H)_2$ ($M = Fe^{II}$ and Mn^{II}).[10] The $C(3)C(4)O_4$ unit is a bis-bidentate ligand to Nd(2) and Nd(3) ions as well as a monodentate ligand to one Nd(1) ion (Figure 5c). Bis-bidentate and monodentate coordination by the same oxalate ligand has not been observed in any metal oxalatophosphates or phosphonates, but has been observed in several metal oxalates.[17] The CH_3PO_3 tetrahedron in **1** shares an edge with

(16) Donnay, G.; Allmann, R. *Am. Mineral.* **1970**, *55*, 1003.

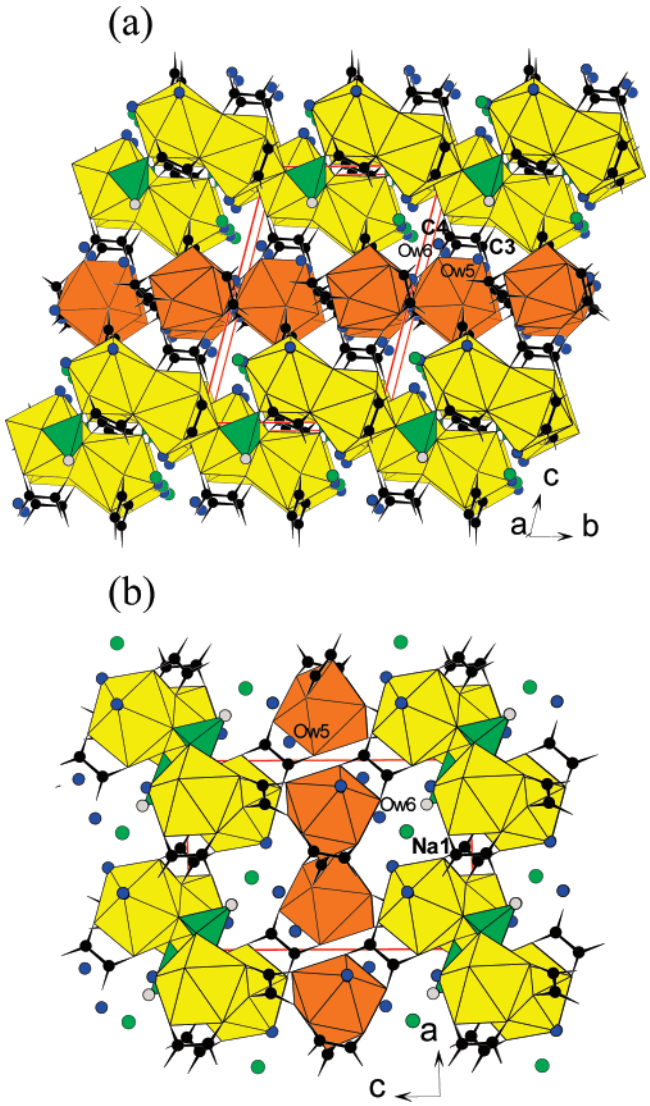

Figure 4. (a) Polyhedral plot of the structure of **1** in a direction approximately parallel to *a*-axis. Key: yellow polyhedra, $Nd(1)O_9$ and $Nd(2)O_9$; brown polyhedra, $Nd(3)O_9$; green tetrahedra, methylphosphonate; blue circles, water O atoms; green circles, Na^+ ions; black circles, oxalate C atoms; gray circles, methyl C atoms. (b) Structure of **1** viewed along the *b*-axis.

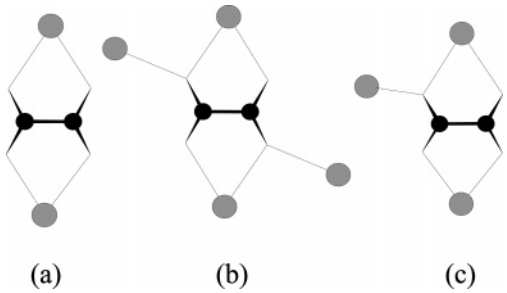

Figure 5. Coordination modes of the oxalate ligands in **1**: (a) bis-bidentate coordination, (b) bis-bidentate and bis-monodentate coordination, and (c) bis-bidentate and monodentate coordination. Key: black circles, oxalate C atoms; gray circles, Nd atoms.

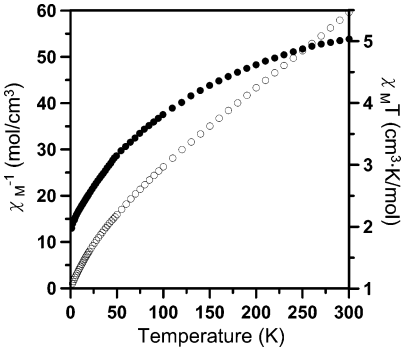

Figure 6. $\chi_M T$ vs T (solid circles) and $1/\chi_M$ versus T (open circles) for **1**.

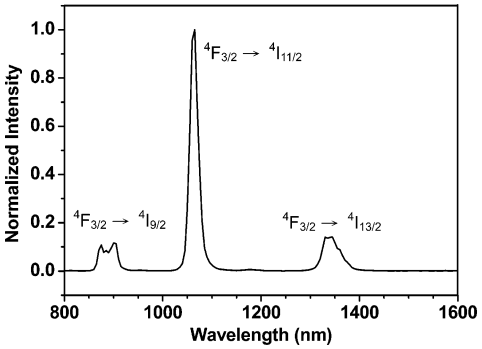

Figure 7. Room-temperature photoluminescence of **1** with excitation at 514.5 nm.

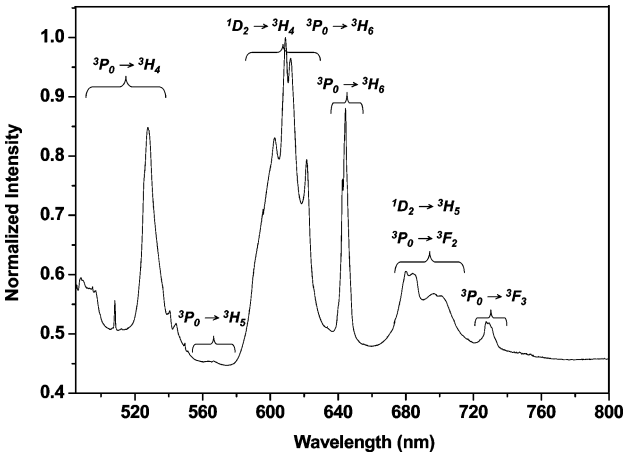

Figure 8. Room-temperature photoluminescence of **2** with excitation at 473 nm.

$Nd(2)O_9$ and coordinates to Nd(1) belonging to an adjacent tetrameric unit. The P−C bond length agrees well with those found in other metal phosphonates. Compound **2** is isostructural with **1** except that the unit cell volume of **2** is larger than that for **1** due to the larger ionic radius of Pr^{3+}.

Magnetic Susceptibility. The free-ion ground state of Nd^{3+} is $^4I_{9/2}$, with the next higher state ($^4I_{11/2}$) at approximately 1900 cm^{-1} higher.[18] The Zeeman factor, g_J, is 8/11 and the theoretical value of $\chi_M T$ for a mononuclear species is 1.64 cm^3 K/mol. The $\chi_M T$ versus T curve for **1** is shown in Figure 6. At room temperature, $\chi_M T$ is equal to 1.68 cm^3 K/mol Nd, which is close to the theoretical value. $\chi_M T$ decreases continuously as T decreases and reaches a value of 0.659 cm^3 K/mol Nd at 2 K. In the 100−300 K range, the magnetic data follow the Curie−Weiss law $\chi_M = C/(T - \theta)$ with $C = 1.73$ cm^3/mol Nd and $\theta = -23.4$ K. The deviation of the magnetic susceptibility with respect to the Curie law results from the crystal field splitting of the $^4I_{9/2}$ state into five doublets. As temperature decreases, the Kramer doublets of higher energy are progressively depopulated and the magnetic susceptibility does not follow Curie law, and only one doublet is populated at 20 K or below. Thus, Nd^{3+} has an effective doublet ground state. The magnetic interactions between the Nd^{3+} ions in the structure are expected to be small.

Photoluminescence. The solid-state photoluminescence spectra of compounds **1** and **2** were recorded at room temperature (RT) and are depicted in Figures 7 and 8, respectively. In Figure 7, the spectrum of **1** shows three infrared emission bands centered at approximately 900, 1060, and 1340 nm ($\lambda_{ex} = 514.5$ nm), which correspond to the $^4F_{3/2} \rightarrow {}^4I_{9/2}$, $^4F_{3/2} \rightarrow {}^4I_{11/2}$, and $^4F_{3/2} \rightarrow {}^4I_{13/2}$ transitions, respectively. The spectrum is analogous to the previously reported spectrum of the coordination polymer $[Nd_2(NDC)_3(DMF)_4]\cdot H_2O$ (NDC = 1,4-naphthalenedicarboxylate).[19] The splitting of the peaks at 900 and 1340 nm can be ascribed to three different neodymium coordination geometries. In contrast to the well-known emission spectrum of Nd(III), the studies of the Pr(III) emission spectrum are much fewer in number. Figure 8 shows the RT emission spectrum of **2** with a 473 nm excitation source. As one can see in Figure 8, unlike the emission spectrum of Nd(III), the spectrum of Pr(III) contains a series of emission bands that cover the entire green to red wavelengths. The peaks observed at 480−540 nm and those at 550−570 nm can be assigned to the $^3P_0 \rightarrow {}^3H_4$ and $^3P_0 \rightarrow {}^3H_5$ transitions, respectively.[20,21] Those peaks between 580 and 650 nm are a mixture of the $^1D_2 \rightarrow {}^3H_4$ and $^3P_0 \rightarrow {}^3H_6$ transitions, whereas those in the range of 670−718 nm correspond to the mixed emissions of $^1D_2 \rightarrow {}^3H_5$ and $^3P_0 \rightarrow {}^3F_2$. In other words, the observed transitions in Figure 8 can be classified to three transition types: $^3P_0 \rightarrow {}^3H_J$, $^3P_0 \rightarrow {}^3F_J$ and $^1D_2 \rightarrow {}^3H_J$ because the 473 nm excitation pumps Pr(III) from the ground $^3H_4$ state to the excited $^3P_0$ state and emission from the $^3P_0$ state or that from the lower $^1D_2$ state due to relaxation can be observed. For the peaks between 580 and 720 nm, we have tried to distinguish the mixed transitions by recording the emission lifetime of every peak in Figure 8, because the lifetime of a triplet−triplet emission should be on the order of 10 μs for Pr(III), but that of a singlet−triplet emission should be on the order of 100 μs.[22] Unfortunately, we found that the

(17) (a) Boudaren, C.; Auffredic, J. P.; Louër, M.; Louër, D. *Chem. Mater.* **2000**, *12*, 2324. (b) Kolitsch, U. *Acta Crystallogr., Sect. C* **2003**, *59*, m501. (c) Chapelet-Arab, B.; Nowogrocki, G.; Abraham, F.; Grandjean, S. *J. Solid State Chem.* **2004**, *177*, 4269. (d) Trombe, J. C.; Mohanu, A. *Solid State Sci.* **2004**, *6*, 1403. (e) Vivas, C. Y.; Delgado, F. S.; Ruiz-Pérez, C.; Julve, M. *CrystEngComm* **2004**, *6*, 11.
(18) Andruh, M.; Bakalbassis, E.; Kahn, O.; Trombe, J. C.; Porcher, P. *Inorg. Chem.* **1993**, *32*, 1616.
(19) Yang, J.; Yue, Q.; Li, G.-Q.; Cao, J.-J.; Li, G.-H.; Chen, J.-S. *Inorg. Chem.* **2006**, *45*, 2857.
(20) Lin, Y.-F.; Chang, Y.-H.; Chang, Y.-S.; Tsai, B.-S.; Li, Y.-C. J. *J. Electrochem. Soc.* **2006**, *153*, G543.
(21) (a) De Mello Donegá, C.; Lambaerts, H.; Meijerink, A.; Blasse, G. *J. Phys. Chem. Solids* **1993**, *54*, 873. (b) De Mello Donegá, C.; Meijerink, A.; Blasse, G. *J. Phys. Chem. Solids* **1995**, *56*, 673.
(22) Gaft, M.; Reisfeld, R.; Panczer, G. *Modern Luminescence Spectroscopy of Minerals and Materials*; Springer-Verlag: Berlin, 2005.

emission lifetime of **2** is always approximately 1.7−2.5 μs. These emission lifetimes are much shorter than the expected values due to the existence of water molecules in this compound. Water molecules (H_2O) and hydroxyl groups (−OH) are well-known for their strong quenching effects on radiative emissions. The same phenomenon was observed in the emission lifetime of **1**, which was measured to be roughly 1.6 μs, but the expected value should be roughly 300 μs. In other words, both compounds show much shorter lifetimes than the expected values[22] due to water molecules as ligands in these compounds. Because of the strong quenching effects, the emission lifetimes in **2** cannot be described by a simple exponential function, and we were unable to distinguish the assignments of mixed emissions from 580 to 720 nm. It should be also noted that Nd(III) and Pr(III) compounds are famous luminescence materials for up-conversion emissions.[19,23] We did attempt to find the up-conversion emissions for these compounds, but in spite of our endeavors, no up-conversion emission signal was found. This lack of up-conversion in these two compounds could be also attributed to the existence of water molecules as ligands, which strongly quench the emissions before any up-conversion mechanism can take place. Although Yang et al.[19] reported a Nd(III) compound containing water has up-conversion emissions, unlike **1** and **2**, the water molecule is not a ligand of Nd(III) in their compound.

In summary, we have synthesized and structurally characterized a new 3D framework neodymium oxalatophosphonate and the praseodymium analogue. Three different types of oxalate coordination are observed in the structure. An unusual bis-bidentate and monodentate coordination by the same oxalate is observed for the first time in metal oxalatophospates or phosphonates. The two compounds are the first examples of lanthanide oxalate-methylphosphonate. The photoluminescence properties of both compounds and the magnetic properties of the neodymium compound have also been studied. The neodymium compound displays characteristic emission bands in the near IR region. The $\chi_M T$ value at room temperature is close to the theoretical value for a mononuclear Nd^{3+} species. The luminescence spectrum of **2** contains many emission peaks that cover the entire green to red wavelengths. The much shorter emission life times of Nd^{3+} and Pr^{3+} in the two compounds than the expected values can be ascribed to the quenching effects of water molecules in the structure.

We have been interested in applying new synthetic methods to the exploratory synthetic and structural studies of new materials with open-framework structures and interesting properties. Recently, we reported the use of a deep eutectic solvent in the synthesis of transition metal oxalatephosphates and phosphonates.[4j,10] A study of the solubility of rare earth metal salts in ionic liquids will be carried out. Investigation into the ionothermal synthesis of lanthanide oxalatophosphonates is in progress.

Acknowledgment. We thank the National Science Council for support and Ms. Chun-Yu Chen and Prof. Sue-Lein Wang at National Tsing Hua University for X-ray data collection.

Supporting Information Available: Crystallographic data for **1** and **2** in CIF format and X-ray powder patterns in PDF format. This material is available free of charge via the Internet at http://pubs.acs.org.

CM070602I

(23) Simura, R.; Jouini, A.; Kamada, K.; Yoshikawa, A.; Aoki, K.; Guyot, Y.; Boulon, G.; Fukuda, T. *J. Cryst. Growth* **2006**, *291*, 309.